

Enhancing graphitic domains by thermally driven structural evolution in graphene oxide

Tobias Foller¹, Xiaoheng Jin¹, Richard Webster², Jeaniffer E. Yap¹, Aditya Rawal², Xinyue Wen¹, Kanishka DeSilva³, Masamichi Yoshimura³, Heriberto Bustamate⁴, Priyank Kumar⁵, Yi You^{1,6} and Rakesh Joshi^{1, *}

¹*School of Materials Science and Engineering, University of New South Wales, Sydney, NSW 2052, Australia*

²*Mark Wainwright Analytical Centre, University of New South Wales, Sydney, NSW, 2052, Australia*

³*Surface Science Laboratory, Toyota Technological Institute, Nagoya 468-8511, Japan*

⁴*Sydney Water, Parramatta, New South Wales 2125, Australia*

⁵*School of Chemical Engineering, University of New South Wales, Sydney, NSW, 2052, Australia*

⁶*School of Physics and Astronomy, University of Manchester, Manchester M13 9PL, UK*

**email: r.joshi@unsw.edu.au*

Graphene oxide (GO) holds high potential for various applications due to its extraordinary properties as well as easy scalability and functionalization. Particularly, thermally driven structural evolution in GO might play a key role in enhancing and controlling its properties. Numerous experimental studies use this evolution to tailor GO and it was predicted through various theoretical studies. However, there is still a lack of direct experimental observation and these findings rely on modelling or indirect conclusions. Here, we present an extensive transmission electron microscopy study backed by structural and chemical analysis as a first direct observation of the thermally driven structural evolution. It is shown that graphitic domains dramatically increase including areas over 200 nm². This change can be attributed to the thermally driven agglomeration of functional groups. In good agreement with previous theoretical predictions, this process is combined with a slight decomposition and composition changes in functional groups. Furthermore, the crucial role of this phenomenon for the room temperature stability of GO is confirmed and a so far unnoticed role of the environment on the agglomeration process is revealed.

Graphene oxide (GO) is a versatile material with a broad spectrum of possible applications such as water purification, gas separation, energy storage, and energy harvesting^{1–8}. This is not only attributed to its superior properties but especially to the easy handling and scalability^{9–11}. Despite its promising nature, various challenges must be overcome in the same scalable manner to push GO to the next step towards an industrial impact. In that sense, mild thermal treatment of GO revealed itself as a powerful and scalable tool as it leads to substantial increase in electrical conductivity, adsorption in the visible region¹², facilitation of cell capture¹³, high increase in capacity¹⁴, as well as in mechanical strength¹⁵ and the possibility to tailor the outcome of subsequent reduction⁵. These studies explain the improvements by

a thermally driven agglomeration of the functional groups on the GO basal plane as follows. Mild temperatures (around 80 °C) allow the functional groups to diffuse and cluster. As a consequence a pronounced ordering of the sp^2/sp^3 phase (graphitic/functionalized domains) is achieved, increasing the size of graphitic domains without compromising with the oxygen content^{5,12–14,16}. According to theory, this mechanism is regarded as essential for the room temperature stability of GO^{17,18}. Moreover, various theoretical works support facile diffusion and energetically favourable clustering of oxygen functionalities^{5,12–14,16–21}. Despite its importance from a fundamental science as well as potential application point of view, there is still a lack of a direct experimental observation of the oxygen clustering in GO upon mild thermal treatment.

In this study, an extensive transmission electron microscopy (TEM) study on monolayer GO is conducted and the clustering of the oxygen functionalities is observed. A comparison of heat treatment in air and vacuum reveals its dependence on the environmental conditions, neglected by the literature so far. The findings are further supported by an extensive chemical and structural analysis, especially solid state nuclear magnetic resonance (SSNMR) measurements. Patches of GO covered TEM grids, GO powder, and GO films were heat treated in vacuum and air at 80 °C for several days. The temperature of 80 °C was chosen as previous studies indicate that this temperature is optimal for the agglomeration process^{5,12–14,16}. It is below the decomposition temperature of functional groups and leads to most prominent changes in the properties of GO¹².

Results

It is possible to classify TEM images of GO monolayer into high contrast and disordered areas containing oxygen functionalities and low contrast and ordered areas representing graphitic domains^{22,23}. Therefore, by TEM imaging the state and distribution of the sp^2/sp^3 phase can be directly observed. Fig. 1 A1-2, exemplary show a comparison of TEM images of untreated GO monolayer and heat-treated GO (80 °C, 14 days in air). For clarity, well-ordered areas (graphitic domains) have been marked in light blue while disordered areas (functionalized areas) remain in grey colour. Since this distinction is only possible in monolayer GO, only monolayer regions were taken into account for the analysis. The identification of monolayer regions is described in supplementary Fig. S1. Consistent with previous studies²², the untreated GO show graphitic domains with a size of mainly 1-10 nm². However, the 14 days samples show fewer and larger graphitic areas with sizes up to 200 nm². Therefore, the heat-treated GO shows a

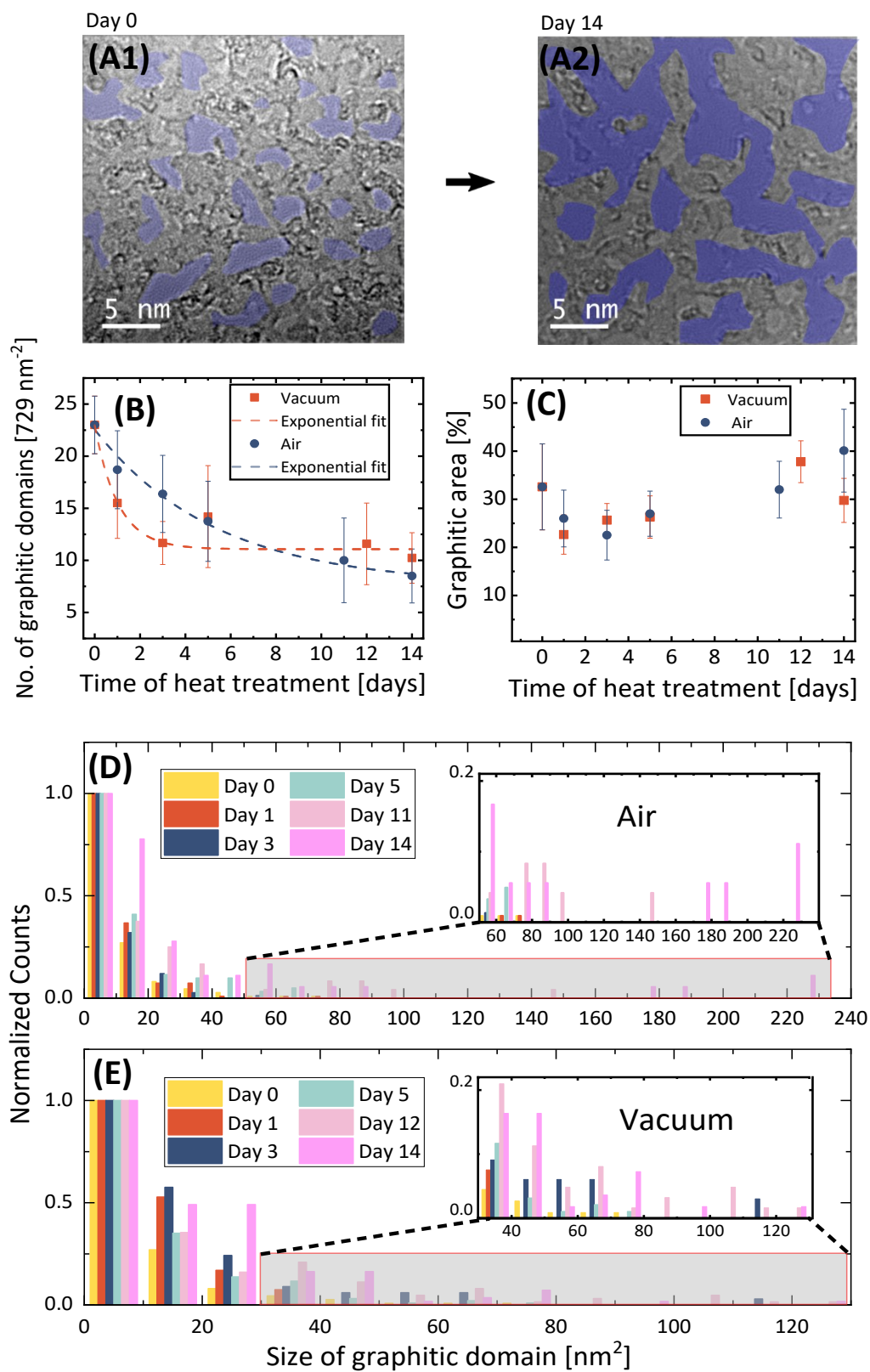


Figure 1 TEM study of heat treatment in air and vacuum (A1+2) TEM image of untreated and 14 days heat treated monolayer GO in air. Graphitic domains are marked in light blue (B) Exponential decay of the **number** of separate graphitic domains (C) Average **percentage coverage** of graphitic area (D, E) Histograms of the **size distributions** of graphitic domains for increasing days of heat treatment in air and vacuum. Day 0 samples represent the same untreated GO. Error bars for (B) and (C) come from standard deviation averaging over 6-12 images.

clear increase in size of graphitic domains. A time-course for heat treatment in air and vacuum is shown in supplementary Fig. S3 A and B revealing the gradual increase in size of the graphitic domains.

For a representative view of the changes during heat treatment, a statistical approach averaging over 6-12 images per heat treatment day was undertaken. Analysing the development of the number of separate graphitic domains, their size distribution as well as the percentage coverage of graphitic area per image allows to quantify a potential ordering process upon mild thermal heat treatment (see also supplementary Fig. S2 for a description of analysis process). Fig 1, B to E, summarize these findings for heat treatment in air and vacuum. In both environments, the number of graphitic domains per image (27x27 nm) decreases exponentially with time (Fig. 1B). Simultaneously, the average percentage coverage with graphitic area remains constant within the measurement capabilities (Fig. 1C). The histograms in Fig. 1D and 1E of the size distribution show that the size of the graphitic domains subsequently increases with time, giving rise to graphitic domains up to the range of 150-250 nm² after 14 days of heat treatment in air. As mentioned above, such large graphitic domains are not observable in untreated GO. Comparing the heat treatment in air and vacuum reveals that the number of graphitic domains increases faster but saturates quicker in a higher amount of smaller graphitic domains in vacuum than in air.

The observed changes in the graphitic domains could also origin from a removal of adsorbates such as hydrocarbon and physisorbed oxygen as well as from the decomposition of functional groups^{22,24}. The fact that the percentage coverage with graphitic area does not undergo drastic changes under mild thermal treatment (Fig. 1C) and electron exposure (see supplementary Video S1), suggests that the changes do not mainly origin in decomposition of functional groups or removal of adsorbates. However, more subtle changes to the composition and number of functional groups do not lie within the sensitivity of this measurement technique. Therefore, additional chemical and structural analysis of the evolution of GO under mild thermal treatment are performed.

Complementary to the TEM study, GO films fabricated via vacuum filtration and GO powder were structurally and chemically analysed before and after heat treatment. Supplementary Fig. S4 A and B show the FTIR spectra of the GO films annealed in air and vacuum. Generally, the broad peak around 3000-3500 cm⁻¹ is attributed to -OH groups. Between 1618 cm⁻¹ and 1625 cm⁻¹ three peaks overlap from intercalated H₂O, C=C and C=O. The region of 1000 cm⁻¹ and 1300 cm⁻¹ can be assigned to C-O and C-O-C functionals^{12,16,25}. The broad peaks around 3000-3500 cm⁻¹ undergo a change and reduction during the 14 days heat treatment period in air, the peak assigned to C=C gains in intensity. In contrast, the vacuum

heat-treated samples show no changes in the -OH functional groups. However, a slight change in the composition of the C-O and C-O-C functionals is observable. It may be noted, that in both cases the signature of the functional groups remains largely intact.

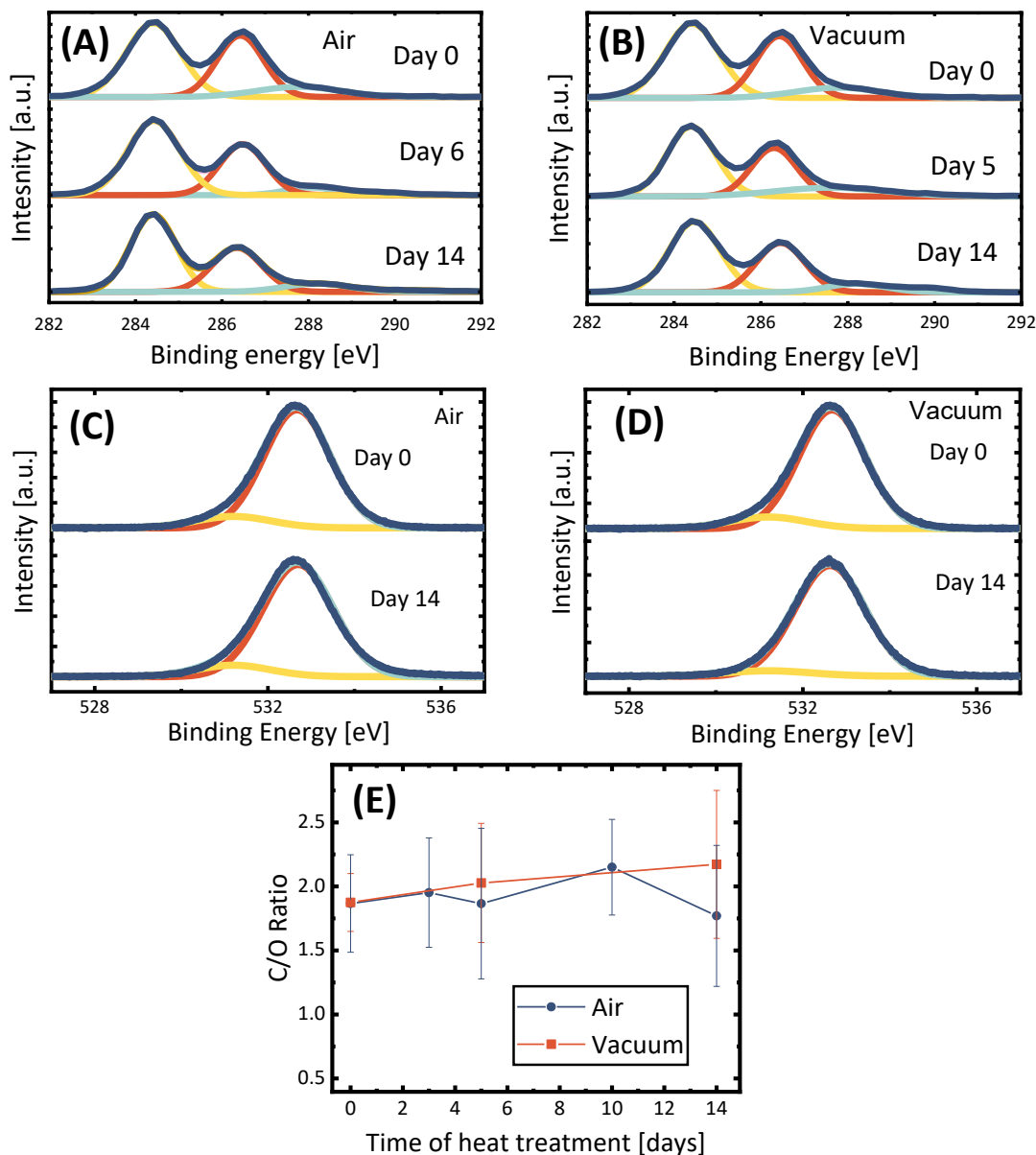
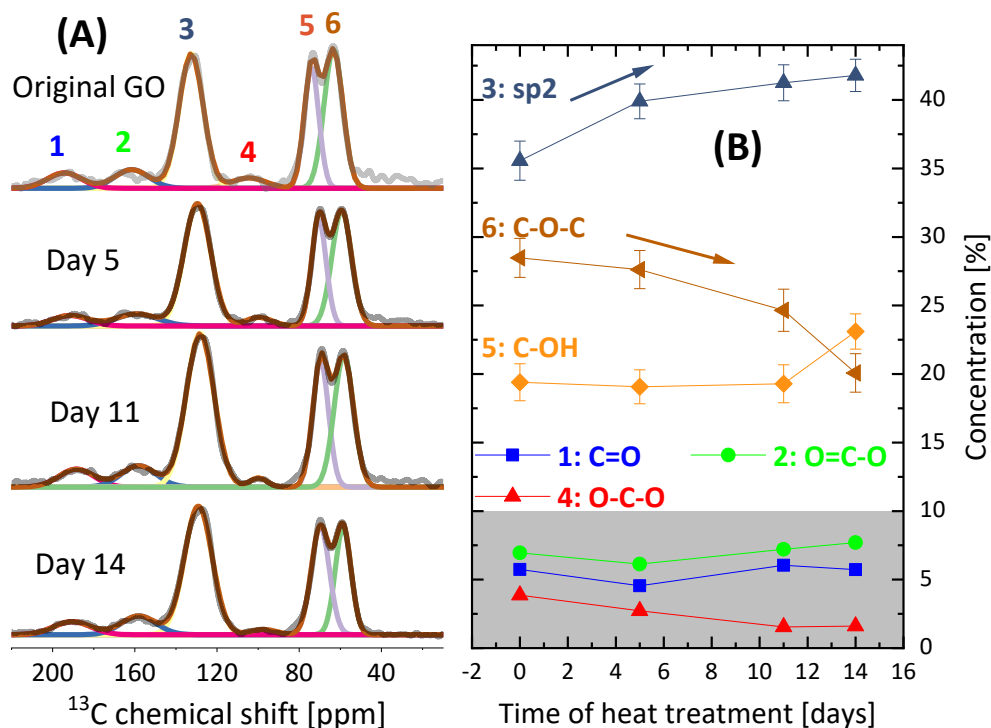


Figure 2 XPS analysis of GO films heat treated in air and vacuum. (A/B) C1s peak development for heat treatment in air/vacuum. (C/D) O1s peak development after heat treatment in air/vacuum. (E) C/O ratio time-course for heat treatment in air and vacuum.

Fig. 2A-E show the XPS spectra over the course of heat treatment. Fig 2A-B show the C1s peak of heat-treated GO in air and vacuum. The results for heat treatment in vacuum are similar. The C-C slightly gains intensity compared to the C-O and C=O during both heat treatment processes. One can see that the

Air



Vacuum

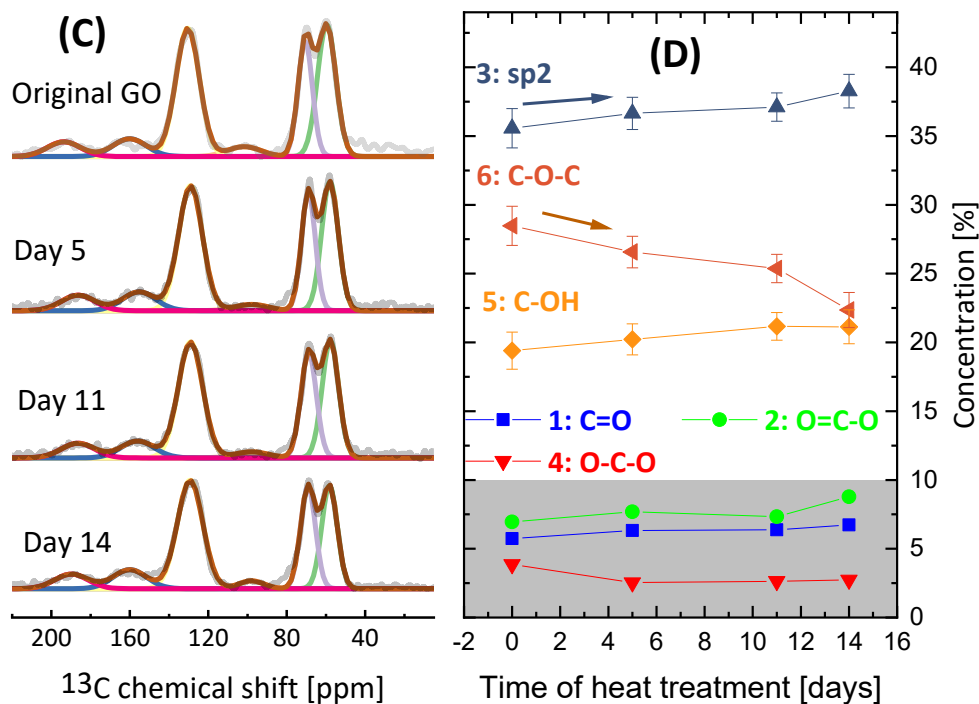


Figure 3 SSNMR study over the time course of annealing. (A) SSNMR spectra of GO annealed in air at 80°C. Peaks 1-6 are assigned following previous studies^{26,27} to 1: C=O, 2: O=C-O, 3: sp²-Carbon, 4: O-C-O, 5: C-OH and 6: C-O-C (B) Concentration of functional groups derived from deconvolutional peak fitting with Gaussian functions of SSNMR spectra for GO annealed in air. (C) SSNMR spectra of GO annealed in vacuum at 80°C (D) Concentration of functional groups derived from deconvolutional peak fitting with Gaussian functions of SSNMR spectra for GO annealed in vacuum. Error bars were depicted from signal to noise ratio. For the Peaks 1, 2 and 4 the ratio is too high and does not allow quantifiable statements, indicated by the grey background.

shape and position of the O1s peak is mostly unaffected by the heat treatments (see Fig. 2 C and D). In line with that, the C/O ratio in Fig. 2E, which also does not significantly change over the time of heat treatment in air and vacuum. The C/O ratios were calculated as a mean value of at least five different survey scans for each sample. The standard deviation results in the given error bars. The slight increase of the C-C peak may be attributed to an increase in graphitic area and the unchanged O1s peak suggests that the chemically bound oxygen remains qualitatively unchanged upon heat treatment in both environments^{12,25}.

To conclude the chemical analysis, Solid State Nuclear Magnetic Resonance (SSNMR) measurements over the course of the heat treatment on dry GO powder were performed. The principal features of all our ¹³C spectra lie in good agreement with GO spectra shown in the literature^{26,27}. Following these studies, the three most prominent peaks around 60 ppm, 70 ppm and 130 ppm are assigned to epoxy, hydroxyl and sp² carbon. The three additional, low intensity peaks are assigned to lactol (~100 ppm), carboxylic acid (~167 ppm) and ketone (~190 ppm) (see Fig. 3A). From deconvolution of the peaks, the development of the relative percentage over the course of heat treatment can be traced. As shown in Fig. 3B an increase of sp² carbon by 6 % over 14 days of heat treatment in air can be observed. It may be noted that the increase is most prominent in the first 5 days and becomes less with ongoing heat treatment. Simultaneously, the relative intensity of the epoxy peak decreases by 7 % and hydroxyl increases by 3 %. For the prominent peaks labelled as 3, 5 and 6 the signal to noise ratio gives an error bar of ~1 %. For the weak intensity peaks from carboxylic acid, ketone and lactol changes are indicated, but the signal to noise ratio does not allow quantifiable statements. Hence, in Fig. 3 B and D their concentrations are represented under a grey area which indicates the sensitivity of the experiment.

In vacuum, the changes in composition of functional groups are less pronounced than in air. The sp² carbon increases by 3 %, while epoxy groups decrease by 6 % and hydroxyl groups increase by 2 %. Similar to treatments in air the weak intensity peaks from carboxylic acid, ketone and lactol changes are indicated, but the signal to noise ratio does not allow quantifiable statements. According to the widely accepted Lerf-Klinowski-model for GO from Hummers' method, epoxy and hydroxyl groups are prominent on the basal plane, while carboxylic acid, ketone and lactol are mostly present on the edges²⁶⁻²⁹. Thus, to investigate the behaviour of functional groups on the basal plane upon heat treatment the latter groups are neglected in the further discussion.

Discussion

To interpret our results, we follow several theoretical and experimental studies suggesting that thermally driven diffusion leads to an energetically favoured agglomeration of oxygen functional groups^{12,14,17–19,21}. This fits well with the observations of our TEM study, as well as chemical and structural analysis. The simultaneous decrease in number and increase in size of graphitic domains suggest that the annealing leads to an ordering process. As possible decomposition of functional groups could also be responsible for increasing the size of graphitic domains observed in TEM, we performed additional control measures and an extensive chemical and structural analysis that will be discussed in the following.

The average coverage with total graphitic area stays stable within the detection limit of our TEM study. The FTIR spectra suggest that the composition of functional groups largely remains constant during the mild thermal treatment. The mostly constant C1s, O1s and C/O ratio, obtained by XPS, further supports that the chemically bound oxygen is only marginally affected by the heat treatment. Since FTIR is not quantitative and XPS only probes the first few nm of the samples, SSNMR measurements were performed. This helps to reduce possible influence of physisorbed oxygen which could lead to a false impression of C/O ratio in XPS¹⁶. Interestingly, the SSNMR spectra reveal a slight increase of sp² carbon by 6 % and 3 %, combined with subtle changes to the composition of functional groups over the course of 14 days heat treatment in air and vacuum. Therefore, all our analytical techniques consistently show that the loss of chemically bond oxygen is marginal compared to the observed large increase in graphitic domain sizes in TEM. Thus, we mainly attribute these changes to the diffusion and agglomeration of functional groups.

A closer look on the SSNMR and TEM results can reveal more details on the nature of the agglomeration process. According to Zhou et al. neighbouring functional groups can form O₂ and H₂O molecules, by decomposition reactions of neighbouring functional groups. However, in clusters of functional groups this decomposition is endothermic and further damped by geometrical factors¹⁷. Thus, the reaction at 80 °C is unlikely and very slow explaining the observed moderate decomposition rate in this study. As it was further predicted by Zhou et al., the most effective low-temperature decomposition is between pairs of epoxy and hydroxyl on the same side of graphene. Consequently, the possibility for those effective pairs to meet would decrease with increasing size of the oxidized areas. Hence, the decomposition probability of functional groups is reduced¹⁷. The correlation between increasing size in oxidized regions (agglomeration), observed in TEM and decreased decomposition rate, observed in SSNMR indicates a

confirmation of this hypothesis. The fact that the decomposition can be primarily attributed to a decrease in epoxy groups underlines the rational of this explanation.

In more detail, previous theoretical and experimental studies^{13,16–20} suggest that the slight decomposition of functional groups after agglomeration is accompanied by a change in the composition of functional groups in the air atmosphere. In SSNMR, we observe a slight increase in hydroxyl groups by 3 %, while the epoxy groups are decomposed by 7 %. This fits well with predictions based on DFT calculations from Kim et al. that the epoxy groups are more prone to decomposition compared to hydroxyl. Moreover, a transition from hydroxyl to epoxy is energetically favoured¹⁸. SSNMR studies on ¹³C-labelled GO could give more insights into the possible role of edge functionalities in this process^{19,20,27}.

The comparison between heat treatment in air and vacuum also supports these findings since the results are similar and thus reproduced. Interestingly, the results differ in detail. According to our TEM results, the enhancement of graphitic domains takes place faster but is less pronounced in vacuum than in air. As shown with our SSNMR analysis, the increase in sp² carbon is less pronounced in vacuum, indicating that the decomposition of functional groups is slower in vacuum than in air. This might contribute to the fact that the observed graphitic domains are larger in air than in vacuum after 14 days of heat treatment. However, it does not explain why the agglomeration in vacuum is slightly faster than in air. Therefore, our observations show, that the diffusion, agglomeration and decomposition process in air and vacuum are different. A detail, that did not get any attention in the literature yet and thus need further experimental and theoretical investigations.

Additionally, we observe a decrease in interlayer spacing that can also be explained by enlarged graphitic areas (see supplementary Fig. S5A). Functional groups in GO act as pillars between two adjacent GO layers³⁰. Upon increasing their distance by agglomeration, larger graphitic areas begin to sag and decrease the average interlayer space. As a side effect, the range of interlayer spaces becomes wider, resulting in an increase in the width of the XRD peak (see supplementary Fig. S5B). Previous studies attributed the decrease in interlayer space to the loss of intercalated water. In this case that might be true to a certain degree as well. However, the more pronounced changes in air than in vacuum contradict with this explanation. We want to add that the observed changes in the composition of functional groups might also play a role in changes of interlayer spacing.

Conclusion

In summary, we present the first direct experimental observation of the thermally driven structural evolution in GO, a phenomenon which was so far only indirectly observed or predicted in theory. We show that the graphitic domains are strongly enlarged while the oxygen content and chemical structure of the functional groups is marginally compromised. However, a slight decomposition and subtle changes in the composition of functional groups are observed, that we can be largely attribute to a decomposition of epoxy groups. By correlating a gradual decrease in decomposition rate to the agglomeration process, it is confirmed that this process contributes to the stability of GO at moderate temperatures in air atmosphere. Additionally, we show that the decomposition and agglomeration of functional groups is influenced by the environment which calls for further investigations.

All in all, this study helps to support various theoretical predictions with experimental data and to understand and control an easily scalable way to enhance the properties of GO films for numerous possible applications.

Materials and methods

Preparation on monolayer GO-TEM grids 10 μ l of the highly diluted and sonicated GO solution was dropped on each TEM grid. By that, a sufficient coverage with mono- and few layer GO was accomplished. Distinguishing between mono- and few layers by analysing the diffraction pattern is straight forward and described in detail in the SI. Between heat treatment and analysis, the samples were stored in a desiccator.

GO films. GO films were fabricated using the vacuum filtration method as described in our previous studies^{3,31,32}. With a pressure of 60 kPa the GO solution was filtrated through a PVDF support membrane. All the GO films have the same average effective size of $\sim 3.0 \text{ cm}^2$. Before further use the films were dried and stored in a desiccator.

Heat treatment in air and vacuum. GO-TEM grids, GO films and powder were annealed in the same conditions in vacuum and air. One batch of samples were placed onto a hot plate at $80 \text{ }^\circ\text{C} \pm 5 \text{ }^\circ\text{C}$ and covered with a glass container. The temperature was constantly monitored with a thermocouple around multiple spots of the samples. Another batch of samples were placed in a vacuum oven at $80 \text{ }^\circ\text{C} \pm 1 \text{ }^\circ\text{C}$. The temperature was also monitored at multiple spots via a thermocouple inside the oven. The base pressure was $3 \cdot 10^{-3} \text{ mbar}$. To remove residual oxygen and moisture, highly purified N_2 was let into the chamber with a mass flow controller so that the pressure is at $1.8 \cdot 10^{-1} \text{ mbar}$. Before initially starting the experiment and after subsequently removing samples from the oven, care was taken that the base pressure was reached and N_2 was let into chamber for at least 30 minutes before start heating again.

Characterization. TEM images were obtained using a JEOL JEM-F200 at 80 kV to avoid damage to the GO. XPS measurements were carried out on an ULVAC-PHI 5000 Versa probe II, with an Al-K α monochromatic X-ray source (energy = 1486.68 eV). C 1s = 284.8 eV for adventitious hydrocarbon was used as binding energy reference. XRD patterns were collected with an Empyrean Thin-Film XRD. FTIR spectra were recorded with a PerkinElmer Spectrum 100/Spotlight 400 in attenuated total reflectance. The ^{13}C nuclear magnetic resonance (NMR) experiments were performed using a Bruker AVANCE III 300 spectrometer, with a 7 Tesla superconducting magnet, operating at frequencies of 300 MHz and 75 MHz for the ^1H and ^{13}C nuclei, respectively. Approximately 40 mg each of sample was centre packed into 4 mm zirconia rotors fitted with Kel-F $^{\circ}$ caps and spun to 12 kHz at the magic angle. The quantitative ^{13}C NMR spectra were acquired with a Hahn-echo sequence to ensure a flat baseline, and 100 s recycle delay to ensure complete signal relaxation. The ^1H decoupling was achieved using a SPINAL-64 with a 71 kHz decoupling field strength, and 768-1024 signal transients were co-added to ensure sufficient signal to noise. The 90 $^{\circ}$ pulse lengths of 4 μs and 3.5 μs were used for the ^{13}C and ^1H nuclei respectively. The Glycine C=O resonance set to 176.4 ppm was used to reference the NRM chemical shifts.

References

1. Loh, K. P., Bao, Q., Eda, G. & Chhowalla, M. Graphene oxide as a chemically tunable platform for optical applications. *Nat. Chem.* **2**, 1015–1024 (2010).
2. Jin, X. *et al.* Effective Separation of CO₂ Using Metal-Incorporated rGO Membranes. *Adv. Mater.* 1907580 (2020). doi:10.1002/adma.201907580
3. Joshi, R. K. *et al.* Precise and Ultrafast Molecular Sieving Through Graphene Oxide Membranes. *Science* (80-.). **343**, 752–754 (2014).
4. Kim, H. W. *et al.* Selective gas transport through few-layered graphene and graphene oxide membranes. *Science* **342**, 91–5 (2013).
5. Kumar, P. V. *et al.* New insights into the thermal reduction of graphene oxide: Impact of oxygen clustering. *Carbon N. Y.* **100**, 90–98 (2016).
6. Zhou, K. G. *et al.* Electrically controlled water permeation through graphene oxide membranes. *Nature* **559**, 236–240 (2018).
7. Li, Z. *et al.* Tuning the interlayer spacing of graphene laminate films for efficient pore utilization towards compact capacitive energy storage. *Nat. Energy* **5**, 160–168 (2020).
8. Wen, Q. *et al.* Electric-Field-Induced Ionic Sieving at Planar Graphene Oxide Heterojunctions for Miniaturized Water Desalination. *Adv. Mater.* **32**, 1903954 (2020).
9. Kong, W. *et al.* Path towards graphene commercialization from lab to market. *Nature Nanotechnology* **14**, 927–938 (2019).
10. Li, D., Müller, M. B., Gilje, S., Kaner, R. B. & Wallace, G. G. Processable aqueous dispersions of graphene nanosheets. *Nat. Nanotechnol.* **3**, 101–105 (2008).

11. Mi, B. Graphene oxide membranes for ionic and molecular sieving. *Science* **343**, 740–742 (2014).
12. Kumar, P. V. *et al.* Scalable enhancement of graphene oxide properties by thermally driven phase transformation. *Nat. Chem.* **6**, 151–158 (2014).
13. Bardhan, N. M. *et al.* Enhanced Cell Capture on Functionalized Graphene Oxide Nanosheets through Oxygen Clustering. *ACS Nano* **11**, 53 (2017).
14. Liu, Z. *et al.* Oxygen Clusters Distributed in Graphene with “Paddy Land” Structure: Ultrahigh Capacitance and Rate Performance for Supercapacitors. *Adv. Funct. Mater.* **28**, 1705258 (2018).
15. Zhang, M. *et al.* Multifunctional Pristine Chemically Modified Graphene Films as Strong as Stainless Steel. *Adv. Mater.* **27**, 6708–6713 (2015).
16. Sun, P. *et al.* Structure evolution of graphene oxide during thermally driven phase transformation: Is the oxygen content really preserved? *PLoS One* **9**, e111908 (2014).
17. Zhou, S. & Bongiorno, A. Origin of the chemical and kinetic stability of graphene oxide. *Sci. Rep.* **3**, 2484 (2013).
18. Kim, S. *et al.* Room-temperature metastability of multilayer graphene oxide films. *Nat. Mater.* **11**, 544–549 (2012).
19. Radovic, L. R., Silva-Tapia, A. B. & Vallejos-Burgos, F. Oxygen migration on the graphene surface. 1. Origin of epoxide groups. *Carbon N. Y.* **49**, 4218–4225 (2011).
20. Radovic, L. R., Suarez, A., Vallejos-Burgos, F. & Sofo, J. O. Oxygen migration on the graphene surface. 2. Thermochemistry of basal-plane diffusion (hopping). *Carbon N. Y.* **49**, 4226–4238 (2011).
21. Suarez, A. M., Radovic, L. R., Bar-Ziv, E. & Sofo, J. O. Gate-voltage control of oxygen diffusion on graphene. *Phys. Rev. Lett.* **106**, (2011).
22. Erickson, K. *et al.* Determination of the Local Chemical Structure of Graphene Oxide and Reduced Graphene Oxide. *Adv. Mater.* **22**, 4467–4472 (2010).
23. Pacilé, D. *et al.* Electronic properties and atomic structure of graphene oxide membranes. *Carbon N. Y.* **49**, 966–972 (2011).
24. Gómez-Navarro, C. *et al.* Atomic structure of reduced graphene oxide. *Nano Lett.* **10**, 1144–1148 (2010).
25. Bagri, A. *et al.* Structural evolution during the reduction of chemically derived graphene oxide. *Nat. Chem.* **2**, 581–587 (2010).
26. Gao, W., Alemany, L. B., Ci, L. & Ajayan, P. M. New insights into the structure and reduction of graphite oxide. *Nat. Chem.* **1**, 403–408 (2009).
27. Cai, W. *et al.* Synthesis and Solid-State NMR Structural Characterization of ¹³C-Labeled Graphite Oxide. *Science (80-.)*. **321**, 1815–1817 (2008).
28. Lerf, A., He, H., Forster, M. & Klinowski, J. Structure of Graphite Oxide Revisited || . *J. Phys. Chem. B* **102**, 4477–4482 (2002).

29. Dreyer, D. R., Park, S., Bielawski, C. W. & Ruoff, R. S. The chemistry of graphene oxide. *Chem. Soc. Rev.* **39**, 228–240 (2010).
30. Nair, R. R., Wu, H. A., Jayaram, P. N., Grigorieva, I. V. & Geim, A. K. Unimpeded permeation of water through helium-leak-tight graphene-based membranes. *Science (80-.).* **335**, 442–444 (2012).
31. Huang, H. H., Joshi, R. K., De Silva, K. K. H., Badam, R. & Yoshimura, M. Fabrication of reduced graphene oxide membranes for water desalination. *J. Memb. Sci.* **572**, 12–19 (2019).
32. You, Y. *et al.* Application of graphene oxide membranes for removal of natural organic matter from water. *Carbon N. Y.* **129**, 415–419 (2018).

Acknowledgements

T.F. acknowledges the UNSW Scientia Ph.D. Scholarship and SSEAU Scholarship. The authors also thank Dr. Shery Chang, Abdul Hakim and Fei Wang for helpful discussion.

Supplementary Information

TEM study

Identification of monolayer GO

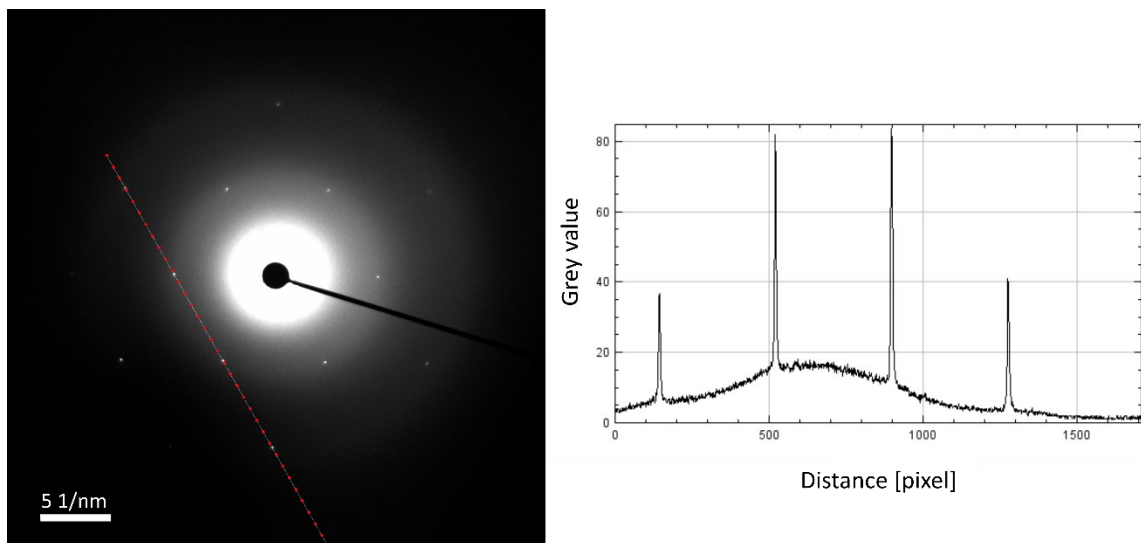


Figure S2 Typical diffraction pattern of the regions used for analysis. It indicates the presence of monolayer GO. A line profile (red dotted line) shows that the $\{1-210\}$ type reflections intensity is lower than the $\{0-110\}$ type reflections intensity. With no significant sample tilt, this suggests the presence of monolayer GO as discussed in previous studies¹⁻³

Development of micrographs upon electron irradiation

Video S1 shows the development of the micrograph of a GO single layer sheet over the course of 80 s. The pictures were taken in two second intervals and the video shows 8 frames per second. Care must be taken in the interpretation of such images, since the distinction between oxygen functional groups and other adsorbates, such as hydrocarbons are not directly possible³⁻⁵. It is apparent that the overall graphitic area does not change significantly over the course of the recorded time. The heating caused by the electron beam leads to movement and desorption of lightly bound adsorbates such as hydrocarbons and physisorbed oxygen on the graphitic areas. If those adsorbates were dominantly present, the exposure would lead to an increase in graphitic area over the time the images are taken^{3,6}. This is not the case. However, movements of the graphitic domain borders and rare creation of holes are observable, matching the argumentation and observation by Erickson et al.³. Some adsorbates might still be bound to the oxidized areas, but this does not compromise with any of the analysis or conclusions

taken in Fig. 1 of the main text since they only rely on the distinction between graphitic domains and functionalized areas.

Analysis of TEM images and statistical approach

For each data point shown in Fig 1B-C in the main text, 6-12 TEM images were acquired and analysed. Supplementary Figure S2 exemplary shows the visual processing of such a TEM image. All images have the same size of 27x27 nm. The graphitic domains are marked in light blue. By converting the image into a black and white image, it becomes processable with the particle analysing function of the software Image J. By that, the total coverage with graphitic area as well as the size distribution and number of separate graphitic domains are recorded and visualized in Fig 1B-E

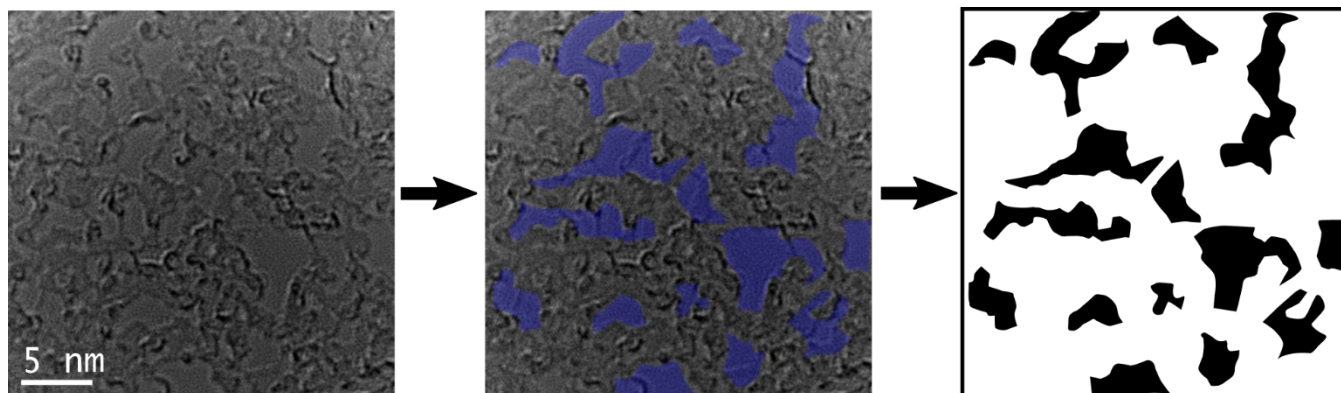


Figure S2 Visual processing of TEM images to obtain average coverage, size distribution and number of graphitic areas

Time-course for heat treatment in air and vacuum

In supplementary Fig. S3, the development of GO during heat treatment in vacuum and air is shown. As stated in the main text, the sample annealed in vacuum show a similar trend as the ones in air. One can see that the graphitic domains increase in size and decrease in number. These types of images are the basis for the results shown in Fig 1 in the main text.

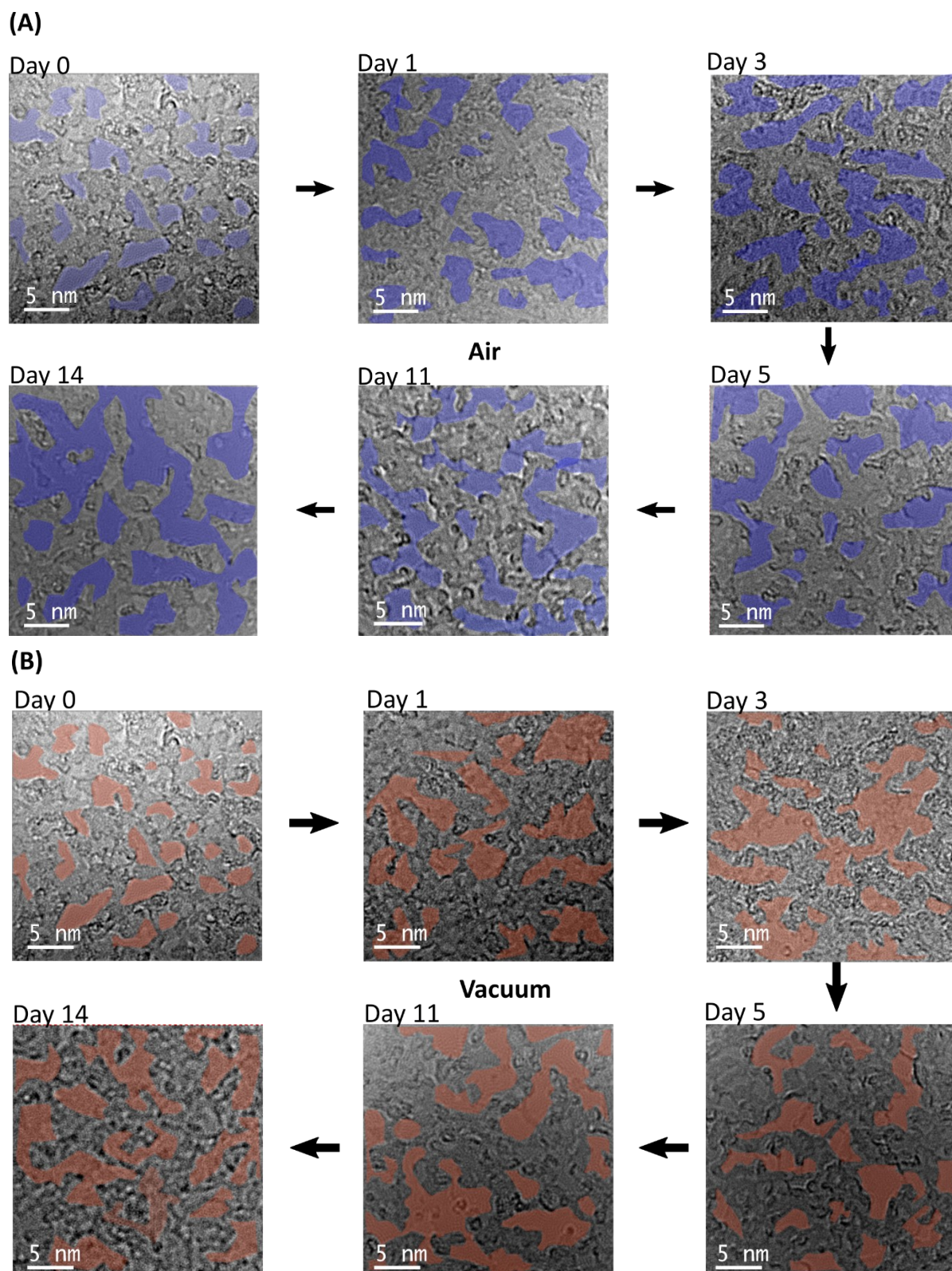


Figure S3 Time course of GO after heat treatment in air/vacuum (A, B). Graphitic domains are marked in light blue/red for treatment in air/vacuum

Supplementary structural and chemical analysis

FTIR

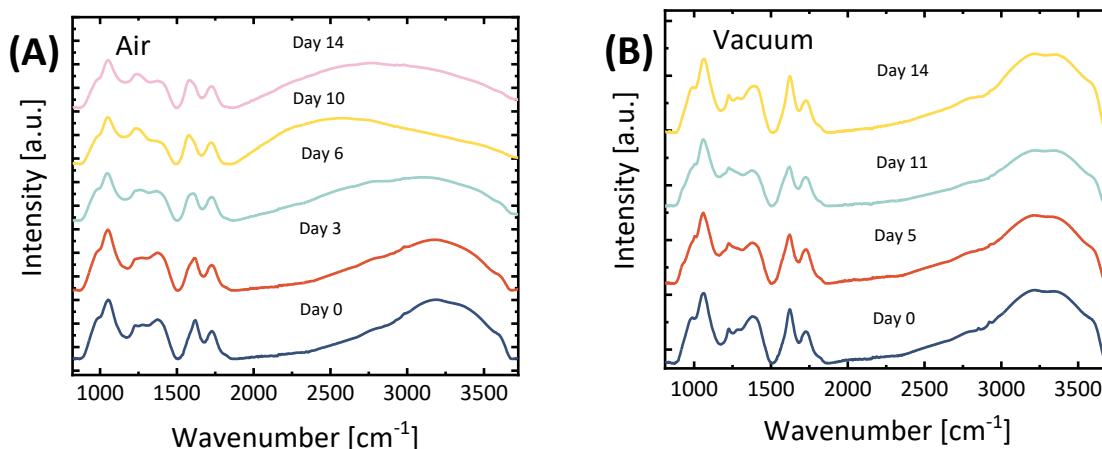


Figure S4 FTIR spectra for heat treated GO films in air and vacuum.

XRD

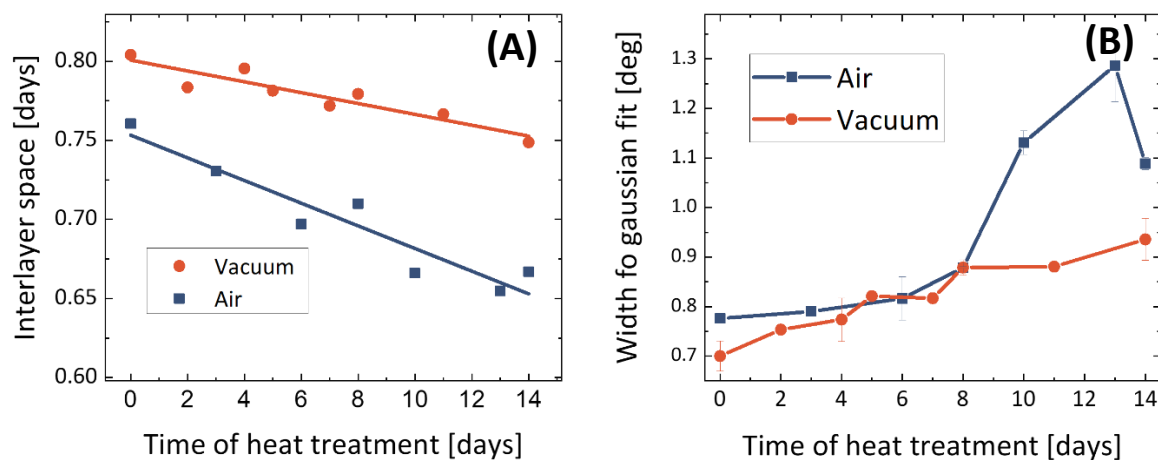


Figure S5 Analysis of XRD pattern over the course of heat treatment in air and vacuum.

Fig. S5A shows the development of the interlayer space upon heat treatment in vacuum (red) and air (blue). Each dot was measured by fitting the (001) peak of the XRD spectrum recorded for each sample. The angle 2θ was then converted into an interlayer space by using Bragg's law and the X-ray wavelength of 1.54 Å.

Both heat treatments result in a smaller interlayer space. However, the treatment in air leads to a more pronounced reduction in interlayer space, resembling in a difference in interlayer space of about 0.1 nm between vacuum and air treated samples after 14 days of heat treatment. Moreover, as shown in Fig.

S5B, the width of the corresponding gaussian fits increase in air and vacuum with a stronger increase in air treatment.

References

1. Meyer, J. C. *et al.* On the roughness of single- and bi-layer graphene membranes. *Solid State Commun.* **143**, 101–109 (2007).
2. Wilson, N. R. *et al.* Graphene Oxide: Structural Analysis and Application as a Highly Transparent Support for Electron Microscopy. *ACS Nano* **3**, 2547–2556 (2009).
3. Erickson, K. *et al.* Determination of the Local Chemical Structure of Graphene Oxide and Reduced Graphene Oxide. *Adv. Mater.* **22**, 4467–4472 (2010).
4. Pacilé, D. *et al.* Electronic properties and atomic structure of graphene oxide membranes. *Carbon N. Y.* **49**, 966–972 (2011).
5. Gómez-Navarro, C. *et al.* Atomic structure of reduced graphene oxide. *Nano Lett.* **10**, 1144–1148 (2010).
6. Meyer, J. C., Girit, C. O., Crommie, M. F. & Zettl, A. Imaging and dynamics of light atoms and molecules on graphene. *Nature* **454**, 319–322 (2008).